Nano Energy 108 (2023) 108248

Contents lists available at ScienceDirect

Nano Energy

journal homepage: www.elsevier.com/locate/nanoen

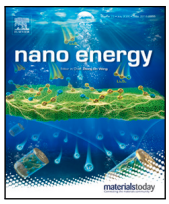

Full paper

Enhancing the acoustic-to-electrical conversion efficiency of nanofibrous membrane-based triboelectric nanogenerators by nanocomposite composition

Wenhao Sun [a,1], Guosheng Ji [b,1], Junli Chen [a], Dan Sui [a], Jie Zhou [a,*], John Huber [b,*]

[a] School of Aeronautics, Northwestern Polytechnical University, Xi'an, 710072, China
[b] Department of Engineering Science, University of Oxford, Parks Road, Oxford, OX1 3PJ, UK

ARTICLE INFO

Keywords:
Nanocomposite membrane
Acoustic
Triboeffect
Energy harvesting

ABSTRACT

Acoustic energy is difficult to capture and utilise in general. The current work proposes a novel nanofibrous membrane-based (NFM) triboelectric nanogenerator (TENG) that can harvest acoustic energy from the environment. The device is ultra-thin, lightweight, and compact. The electrospun NFM used in the TENG contains three nanocomponents: polyacrylonitrile (PAN), polyvinylidene fluoride (PVDF), and multi-walled carbon nanotubes (MWCNTs). The optimal concentration ratio of the three nanocomponents has been identified for the first time, resulting in higher electric output than a single-component NFM TENG. For an incident sound pressure level of 116 dB at 200 Hz, the optimised NFM TENG can output a maximum open-circuit voltage of over 120 V and a short-circuit current of 30 μA, corresponding to a maximum areal power density of 2.25 W/m^2. The specific power reached 259 μW/g. The ability to power digital devices is illustrated by lighting up 62 light-emitting diodes in series and powering other devices. The findings may inspire the design of acoustic NFM TENGs comprising multiple nanocomponents, and show that the NFM TENG can promote the utilisation of acoustic energy for many applications, such as microelectronic devices and the Internet of Things.

1. Introduction

With the rapid growth of urbanisation, excessive airborne noise can seriously harm human health and disrupt people's daily activities [1,2]. Specifically, aeroplane noise, as high as 130 dB, poses a significant threat to airport ground crews and can potentially induce hearing loss [3]. Numerous efforts have thus been made to reduce noise pollution in the environment [2,4–6]. However, from another point of view, noise is an energy source that, with proper design, may be harvested to power small electronic devices. Acoustic energy harvesting is still in its early stages due to its low energy density, poor harvesting ability at low frequencies, and inefficient materials and structures [7–9].

Consequently, developing an ultra-thin, lightweight, and compact device for sound energy harvesting is a promising research direction. Electromagnetic, piezoelectric, triboelectric and ferroelectric effects have all been explored [9–16]. Most electromagnetic acoustic energy harvesters have low voltage outputs, but resonators have been added to these devices to improve their performance [17,18]. Recent research has shown that the performance of piezoelectric sound energy harvesters has significantly improved, but their electrical output remains very low [13,19–29]. Sound energy harvesting devices that use the triboelectric effect can produce renewable electricity based on repeated contact and separation of two dielectric surfaces [20]. As an emerging technology, the triboelectric nanogenerator (TENG) has attracted a great deal of attention due to its ability to generate a considerable amount of electrical power while demonstrating exceptional robustness, cost-effectiveness, and sustainability [30–41].

There are two major aspects of the research being conducted on acoustic nanofibrous membrane (NFM) TENGs. On the one hand, research mostly focuses on strengthening the device structures to increase the electrical output of the acoustic TENG. Despite the majority of research yielding a substantial amount of electrical output, the TENG device structures demand greater mass and space as a tradeoff. For instance, using a Helmholtz cavity, a thin-film nanogenerator based on triboelectrification may achieve a much higher electrical power. However, its volume is substantial with a complex narrow air neck, leading to a low areal power density [12]. Similarly, Cui et al. [42]

* Corresponding authors.
E-mail addresses: jiezhou@nwpu.edu.cn (J. Zhou), john.huber@eng.ox.ac.uk (J. Huber).
[1] Wenhao Sun and Guosheng Ji contributed equally to this work.

https://doi.org/10.1016/j.nanoen.2023.108248
Received 13 December 2022; Received in revised form 16 January 2023; Accepted 28 January 2023
Available online 31 January 2023

Table 1
Triboelectric performance of acoustic TENGs with single nanofibrous membranes.

Matrix	Component	V_{oc} (V)	J_{sc} (mAm^{-2})	Size (cm^2)	Freq. (Hz)	SPL (dB)	Power (Wm^{-2})	Specific power (μWg^{-1})	Refs
PVDF-TrFE	MWCNTs	34.4	0.52	33.16	150	115	0.01162	NG	[8]
PU/PVDF	–	102	0.408	25	NG	NG	0.0416	NG	[51]
PVDF-TrFE	–	14.5	23.75	12	210	115	0.118	NG	[26]
PTFE	–	NG	NG	NG	250	117	0.121	NG	[7]
PAN	–	58	10	12	230	117	0.1753	NG	[52]
PVDF	–	90	45	100	160	114	0.202	NG	[42]
PVDF	PAN	94.1	14.5	12	250	117	0.2501	NG	[28]
PVDF	Mustard seed	84	NG	9	NG	NG	0.334	NG	[53]
PVDF	PDMS	105.5	1.67	100	150	117.6	0.92	NG	[38]
PEP	–	132	6.0	53.29	70	85.3	NG	NG	[44]
PVDF	PAN/MWCNTs	126.5	48.32	6.25	200	116	2.25	259	This work

NG: Not Given; Open-circuit voltage V_{oc}; Short-circuit current density J_{sc}.

achieved high power output from an airborne acoustic TENG by using an electrospun polyvinylidene fluoride (PVDF) film, but the device volume was also high. The integrated TENG proposed by Liu et al. [43] has sandwiched and three-dimensional structures, which can provide several hundred volts of output. However, this multi-layer TENG has high structural complexity and working area. Relevant studies also turn up more devices similar to these, with complex or heavy structures that may cause problems in practical applications [31,44–46]. On the other hand, acoustic TENG studies focus on making lightweight, compact structures; however, it is challenging to achieve high electrical output and low weight simultaneously. Yu et al. [38] claimed that a nanofiber-based acoustic energy harvester with a small size is capable of achieving a relatively high area power density. In addition, compact and lightweight composite aerogel acoustic nanogenerators [8] and paper-based simple TENGs [7] have been explored, but their electrical outputs are limited [47–50].

In light of the above discussion, it is difficult to develop acoustic TENGs with both lightweight structure and high electrical output. As shown in Table 1, there are therefore few references that address both high electric power output and low structural weight. In real applications, the high specific power or power-to-weight ratio, defined as the ratio between electric power output and structural weight, is a dominant measure of performance for powering electronics. Thus, it is worthwhile to develop ultrathin, lightweight, and compact acoustic energy harvesters with high specific power properties. This study proposes a compact nanocomposite acoustic TENG with high specific power based on a single NFM with multiple nanocomponents: polyacrylonitrile (PAN), polyvinylidene fluoride (PVDF), and multi-walled carbon nanotubes (MWCNTs). The nanocomposite NFM TENG has significantly improved electrical output compared to a single-component PVDF or PAN TENG. The maximum areal power output can reach 19 times higher than that of PVDF-TrFE NFM TENGs [26] and 13 times higher than that of PAN NFM TENGs [52], showing that electrospun PAN-PVDF-MWCNT NFM TENGs have excellent acoustoelectric conversion capability. The optimal concentration ratio of the three mixed nanocomponents has been identified for the first time. The TENG demonstrates excellent acoustic energy harvesting capability and high specific power of 259 μW/g. Under an acoustic excitation of 116 dB at 200 Hz, the TENG with an effective membrane area of 6.25 cm^2 can produce a maximum open-circuit voltage V_{oc} of 126.5 V and a short-circuit current I_{sc} of 30.2 μA. In addition, the maximum areal power density can reach 2.25 W/m^2. The accumulated acoustic energy can illuminate 62 commercial light-emitting diodes (LEDs). After rectification, the acoustic NFM TENG can directly power a digital electronic device. Therefore, this study includes not only new ideas for the design of an acoustic NFM TENG with both compact and light-weight structures, but also a guide for improving energy conversion efficiency and specific power output for usage in microelectronic devices and the Internet of Things.

2. Experimental setup

2.1. Materials

Polyacrylonitrile (PAN) powder (Mw, 150,000) and polyvinylidene fluoride (PVDF) powder (Mw, 570,000) were purchased from Arkema Chemical Co., Ltd and Sigma-Aldrich, respectively. N, N-Dimethylformamide (DMF) and acetone were purchased from Sinopharm Chemical Reagent Co., Ltd. The multi-walled carbon nanotubes (MWCNTs) were purchased from Shenzhen Suiheng Technology Co., Ltd.

2.2. Preparation of NFMs

To make nanocomposite NFMs, MWCNTs with various weight concentration ratios (0.5 wt%, 1 wt%, 2 wt%, 3 wt%) were initially dispersed in the DMF solvent for 3 h by using ultrasonic waves. The inner diameter of MWCNTs is located around 5 to 8 nm, while the outside diameter is approximately 10 to 15 nm. The nanotube length is between 2 and 8 μm, and their purity exceeds 98%. Then, the mixture (1.4 g in total) of PVDF and PAN powder with a weight ratio of 1:1 was combined with the obtained MWCNT suspensions. By dissolving the mixture of PAN, PVDF and MWCNTs into a solvent of DMF and acetone at a weight ratio of 7:3, the blended PAN / PVDF / MWCNTs nanocomposite solution was obtained. The solution was stirred at 80 °C for three hours and then cooled to room temperature for electrospinning.

The electrospinning equipment (YFSP-T, Yun fan Technology Co., China.) was used to fabricate nanocomposite NFMs with PAN / PVDF / MWCNT components. For electrospinning, the operating voltage, the feeding rate of the composite solution, the electrospinning distance, the rotational speed of the collector, and the operating temperature were controlled at 15 kV, 2 ml / h, 15 cm, 300 rpm and 38 °C, respectively. Similarly, PAN, PVDF, and PAN/PVDF NFMs were fabricated using the same fabrication technique and parameters, with the exception of the nanocomponent proportions.

2.3. Fabrication of acoustic NFM TENGs

The acoustic NFM TENG was designed as a sandwich structure (size: 4 cm × 4 cm × 1.92 mm). This comprised the NFM (thickness 0.02 mm, effective area 2.5 cm × 2.5 cm), and a 3D printed (Raise 3D Pro2) polylactic acid (PLA) frame/spacer (thickness 1.2 mm), sandwiched between copper mesh electrodes (thickness 0.1 mm), and two polyethylene terephthalate (PET) outside frames (thickness 0.25 mm), as shown in Fig. 1 (a). The NFM and the upper copper mesh was identified as the top triboelectric structure of the NFM TENG. Copper mesh is manufactured by punching copper foils inside specified moulds using a high-speed punching machine. China's Hebei Chaochuang Metal Mesh Industry Co., LTD supplies Cu mesh electrodes with a fibre diameter of 100 μm and an opening area of 1 mm × 2 mm (see Figure S7 in Supplementary). The PLA spacer created a vibration space between the

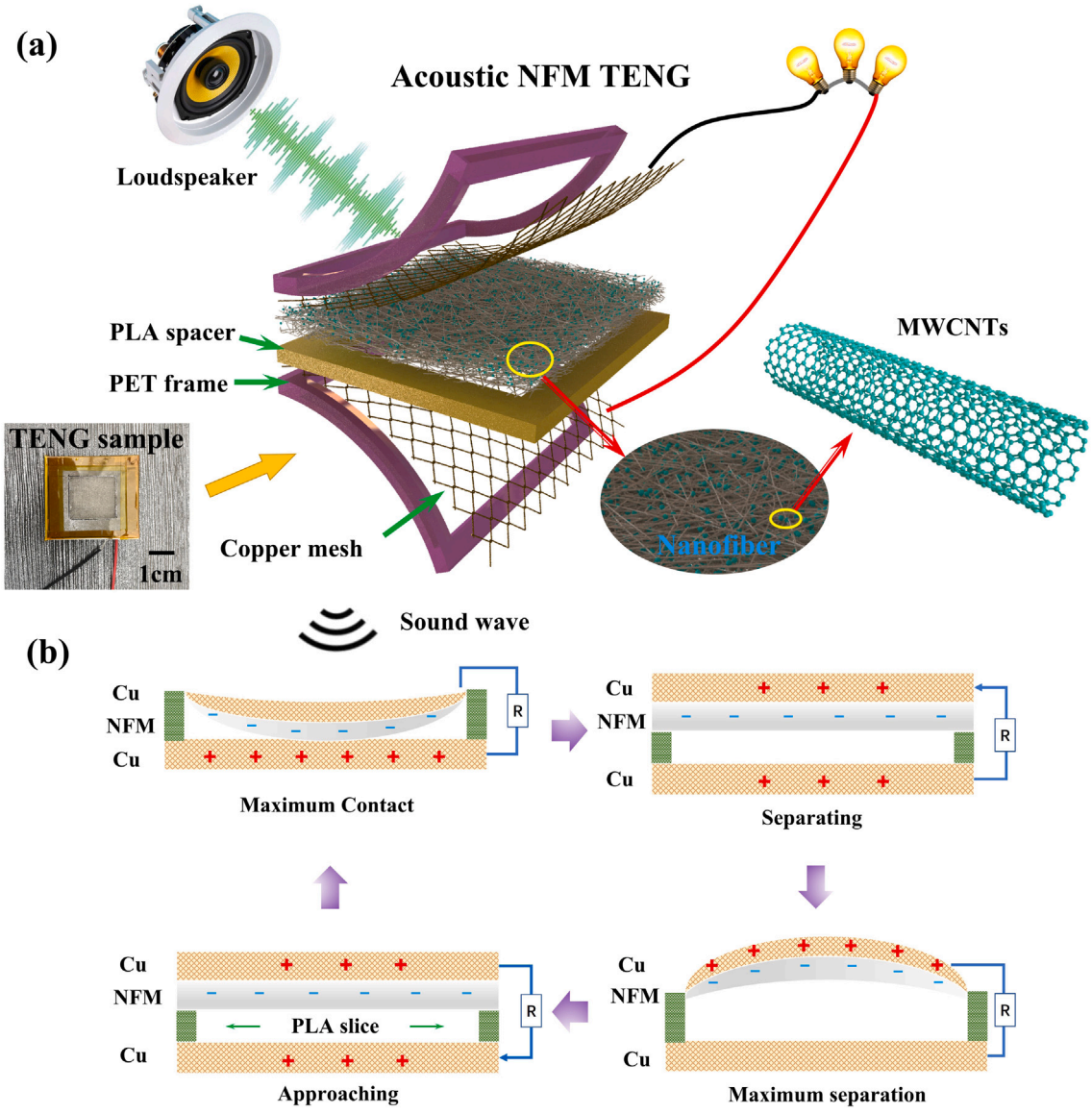

Fig. 1. Schematic diagrams of the acoustic NFM TENG including (a) layer structures and (b) working mechanism.

top triboelectric structure and the lower copper mesh electrode. The two PET outside frames were bound together using insulating tape so as to keep the edge of the NFM in close contact with the upper copper mesh around its edges. Fig. 1 (a) shows the fabricated acoustic NFM TENG with a total mass of 5.45 g (Electronic balance ZG-TP203).

2.4. Characterisation and measurements

The morphology of the nanocomposite NFM was examined using scanning electron microscopy (SEM, Zeiss Supra 55), as given in Figures S1 and S2 (see Supplementary). The nanofiber diameters of all NFMs were measured using Image J. X-ray diffraction (XRD) was obtained using a Panalytical X-ray diffractometer with Cu-Kα radiation in a scanning angle 2θ range of 10–40° at 40 kV and 30 mA (Figure S3 in Supplementary). The FTIR spectra in the ATR mode for the individual materials and their composite material were measured using Thermo Scientific Nicolet iS20 and are shown in Figure S4 of the Supplementary. All samples were scanned from 4000 to 400 cm^{-1} over 32 times for signal averaging. The sound signal is excited at a specific frequency and amplified using a signal generator (Agilent 33220 A) and a power amplifier (Acoustech PA100), respectively. Then a loudspeaker (ETON, 8-412/C8/32) installed in an acoustic impedance tube was adopted as the sound source to stimulate the acoustic TENG. The sound pressure level was measured using a sound level meter (BSWA 308). Additionally, a PXI-4071 National Instruments Digital Multimeter was used to obtain the output voltage and current signals of the acoustic NFM TENGs (see Figure S5 in Supplementary).

3. Results and discussion

The operating mechanism of an acoustic NFM TENG is mostly based on the concept of periodic contact-separation, as shown in Fig. 1 (b). In general, the NFM has a stronger electron affinity than the tribo-positive electrode layer. When the NFM and lower electrode of the TENG come into contact with each other under acoustic pressure, the transfer of surface charges occurs on account of the vast disparity between the NFM and lower electrode in attracting electrons. Specifically, the contact negatively charges the NFM surface owing to its electronegativity while leaving the positive electrode with an equal amount of positive charge. Subsequently, the two contacting surfaces gradually separate from one

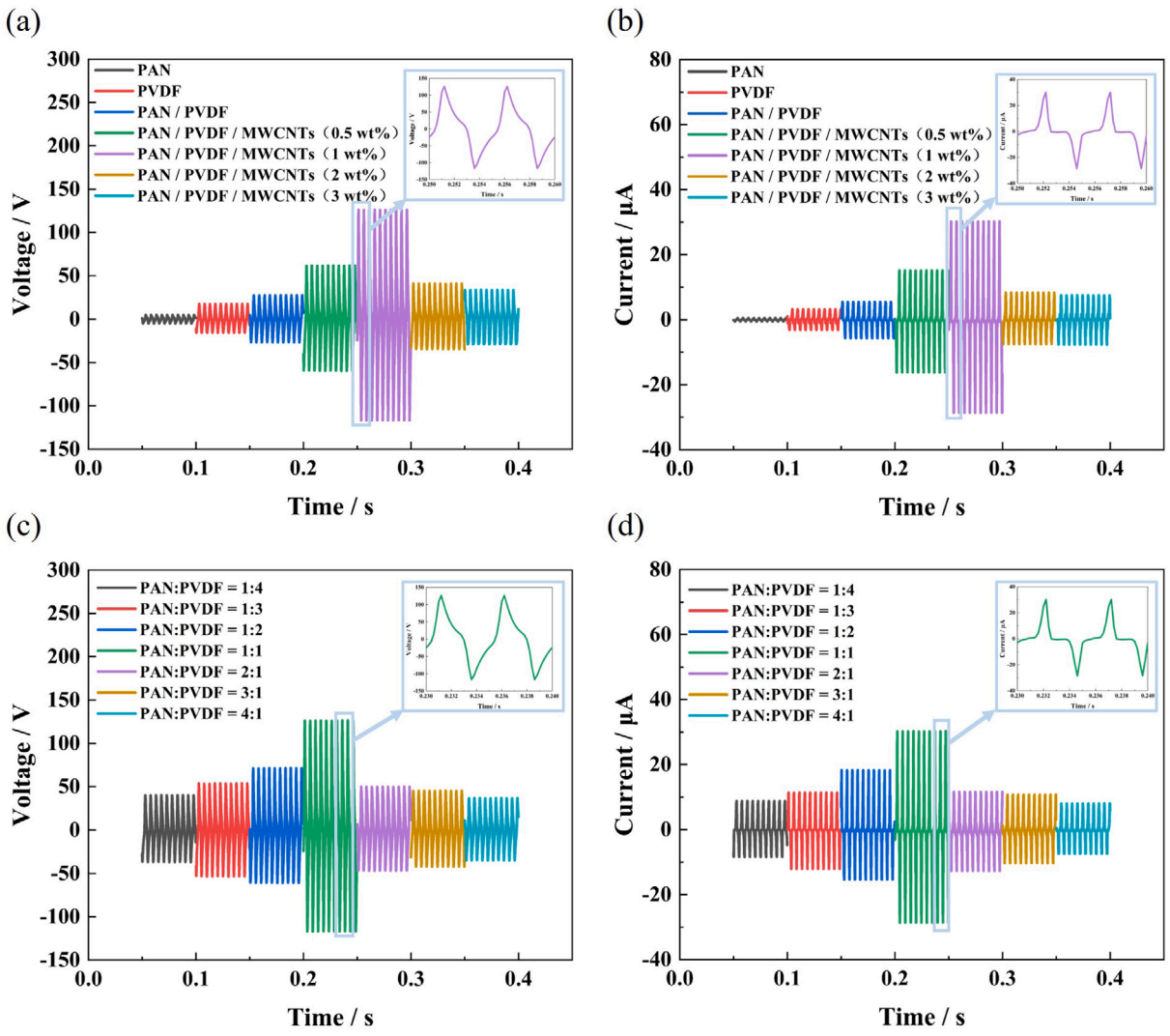

Fig. 2. Acoustic NFM TENGs: (a) open-circuit voltage V_{oc} and (b) short-circuit current I_{sc} for various proportions of PAN, PVDF, and MWCNTs components; (c) open-circuit voltage V_{oc} and (d) short-circuit current I_{sc} for various concentration ratios of PAN and PVDF containing constant weight concentration of MWCNTs (1 wt%).

another due to the changing acoustic pressure, breaking the electrostatic equilibrium. When the NFM separates from the lower electrode in response to the incoming acoustic wave, the opposite triboelectric charge of the two layers forms an electric field between them, which in turn creates a potential difference between the upper and lower electrodes. The free electrons are thus forced to flow from the lower electrode to the upper electrode through the external circuit. Positive charge accumulates on the upper electrode to maintain the equilibrium of the local electric field. Upon the approach of two triboelectric layers, the process is reversed, and electrons move in the other direction. Periodic contact and separation result in alternating current as the acoustic wave propagates.

To assess the acoustic-to-electric conversion performance, an amplitude- and frequency-adjustable loudspeaker was used to excite the acoustic NFM TENG. Firstly, the open circuit voltage, V_{oc}, and short circuit current I_{sc}, were studied using various NFMs, including PAN, PVDF, PAN-PVDF, and PAN-PVDF-MWCNTs with various MWCNT weight concentrations (0.5 wt%, 1 wt%, 2 wt%, 3 wt%). Figure S11 in Supplementary shows the open-circuit voltage of NFM TENGs with PAN-PVDF-MWCNT (1 wt%) components and its corresponding incident acoustic pressure signal. The waveforms of short-circuit current signal over one period for various NFM TENGs are shown in Figure S12 in Supplementary.

The compositions of PAN and PVDF are adjusted while the NFM thickness remains constant to examine the function of PAN and PVDF in the NFM friction layer. All samples made up of various PAN-PVDF compositions had a distinct morphology without any beads (see the SEM images in Figure S1). Fig. 2(a) and 2(b) depict the voltage and current outputs of the NFM TENG under settings of 116 dB SPL and 200 Hz. The NFM TENG constructed from PAN nanocomponents had peak voltage and current outputs of 5.06 V and 0.53 μA, respectively, whereas the NFM TENG made of PVDF nanocomponents had higher peak outputs of 17.5 V and 3.2 μA, respectively. Intriguingly, maximum output (27.6 V and 5.5 μA) was observed with equal amounts of PAN and PVDF. PAN-PVDF NFM TENGs exhibit peak voltage and current outputs that are higher than their single-component equivalents. It implies that PAN and PVDF have a synergistic impact inside the NFM.

In general, when the PVDF composition increases, the PVDF β phase content falls, whereas the PAN zigzag conformation content fluctuates [28]. Due to the strong intermolecular interactions between PAN and PVDF, the electrospun PAN-PVDF NFM had a higher β phase content. XRD and FTIR peak analysis in Figures S3 and S4 reveal the influence of nanocomponents on the β phase content in Table S2 of Supplementary. The significant rise in electric outputs is due to the increase in dipole moments, especially when PAN and PVDF nanocomponents are equal [28]. In addition, frequent interactions between PAN and PVDF components in the condition of acoustic waves

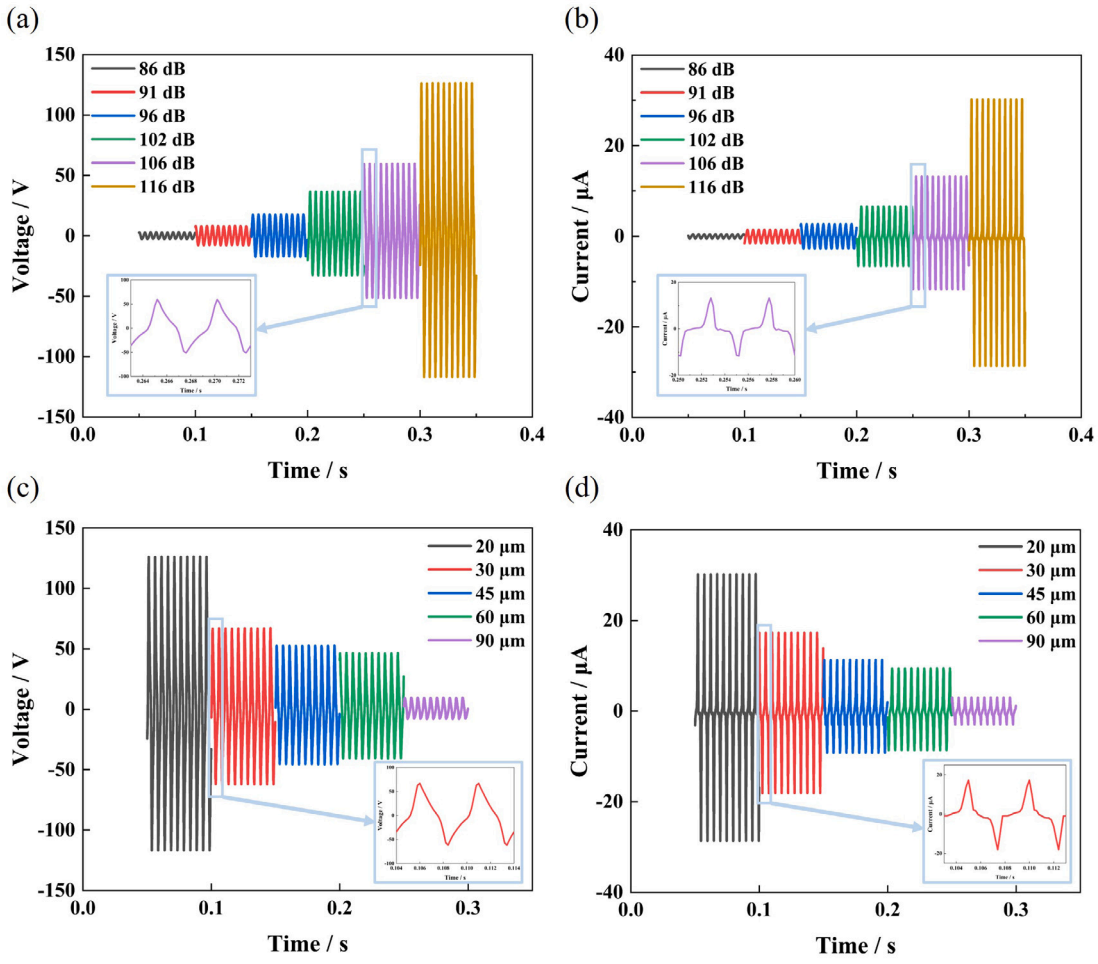

Fig. 3. Nanocomposite acoustic NFM TENGs with PAN-PVDF-MWCNTs (1 wt%) components: (a) open-circuit voltage V_{oc} and (b) short-circuit current I_{sc} for samples under various SPLs; (c) open-circuit voltage V_{oc} and (d) short-circuit current I_{sc} for samples with various NFM thickness.

contribute to the electric outputs of NFM TENGs. Taking into account the triboelectrification mechanism, PVDF is more efficient than PAN materials in attracting electrons. Therefore, the mechanisms of contact and separation between PVDF and PAN nanocomponents result in positive PAN domains and negative PVDF domains. The strong endogenous triboelectric contribution between the nanocomponents of PAN and PVDF leads to high electrical outputs [28]. However, such an endogenous triboelectric effect is rarely observed in PVDF or PAN nanofibers with solo component.

Consequently, the function of PAN and PVDF inside the NFM friction layer is demonstrated below. Firstly, the frequent interaction and deformation of diverse nanofibers inside the NFM generates piezoelectric polarisation on the surface of the fibres. Secondly, the frequent oscillation of the nanofibers causes frequent contact and separation between the PAN and PVDF regions, hence creating an endogenous triboelectric effect due to the triboelectrification difference [28]. Thirdly, the triboelectric effect between PAN-PVDF NFM and electrode layers generates electric outputs. However, the endogenous triboelectric effect cannot occur in single nanocomponent PAN or PVDF NFM TENGs, leading to weakened electrical outputs.

The electrical output of the nanocomposite fibrous-based TENG with PAN-PVDF-MWCNTs components was observed to be greater than that of the single-material NFM TENGs with only PAN or PVDF components in experimental measurements, as given in Fig. 2 (a) and 2 (b). This is most likely due to the fact that bead-like protrusions on the nanofibers, as seen in Figures S1 and S2, provide improved opportunities for contacting with the copper electrodes, resulting in greater triboelectric output. The surface modification increases the surface roughness of electrospun membranes, hence increasing their effective contact area [28]. The MWCNTs also have the ability to raise the β polar phase content in the PVDF nanofibrous matrix in Table S2 of Supplementary. The dielectric polarisation enhances the electron gain or loss performance of the triboelectric surface, hence influencing the charge density [54–56]. In addition, the electric output of the nanocomposite fibrous-based TENG including PAN-PVDF-MWCNT components varied non-monotonically as the concentration of MWCNTs increasing. The MWCNTs increased the membrane's conductivity at low MWCNT concentrations (here 0.5 wt% in Fig. 2 (a) and 2 (b)), as shown in Figure S8, which might improve electron conduction within the membrane and thus enhance the electrical output. However, once the MWCNT content exceeds a specified level, such as weight concentration over 1 wt% in Fig. 2 (a) and 2 (b), the NFM may become too electrically conductive, resulting in a reduction of the TENG's electrical output. The optimum concentration ratio of the three nanocomponents is identified here for the first time: the nanocomposite NFM TENG with PAN-PVDF-MWCNTs (1 wt%) composition demonstrated the greatest electrical output. This TENG achieved a maximum V_{oc} of 126.5 V and I_{sc} of 30.2 μA.

Next, the electrical outputs of nanocomposite NFM TENGs containing PAN-PVDF-MWCNTs components were examined with varying concentration ratios between PAN and PVDF, as given in Fig. 2 (c) and 2 (d). The results indicate that the electrical outputs of the nanocomposite NFM TENG are not linearly linked to the concentration level of PAN or PVDF. The optimal ratio between PAN and PVDF was found to be

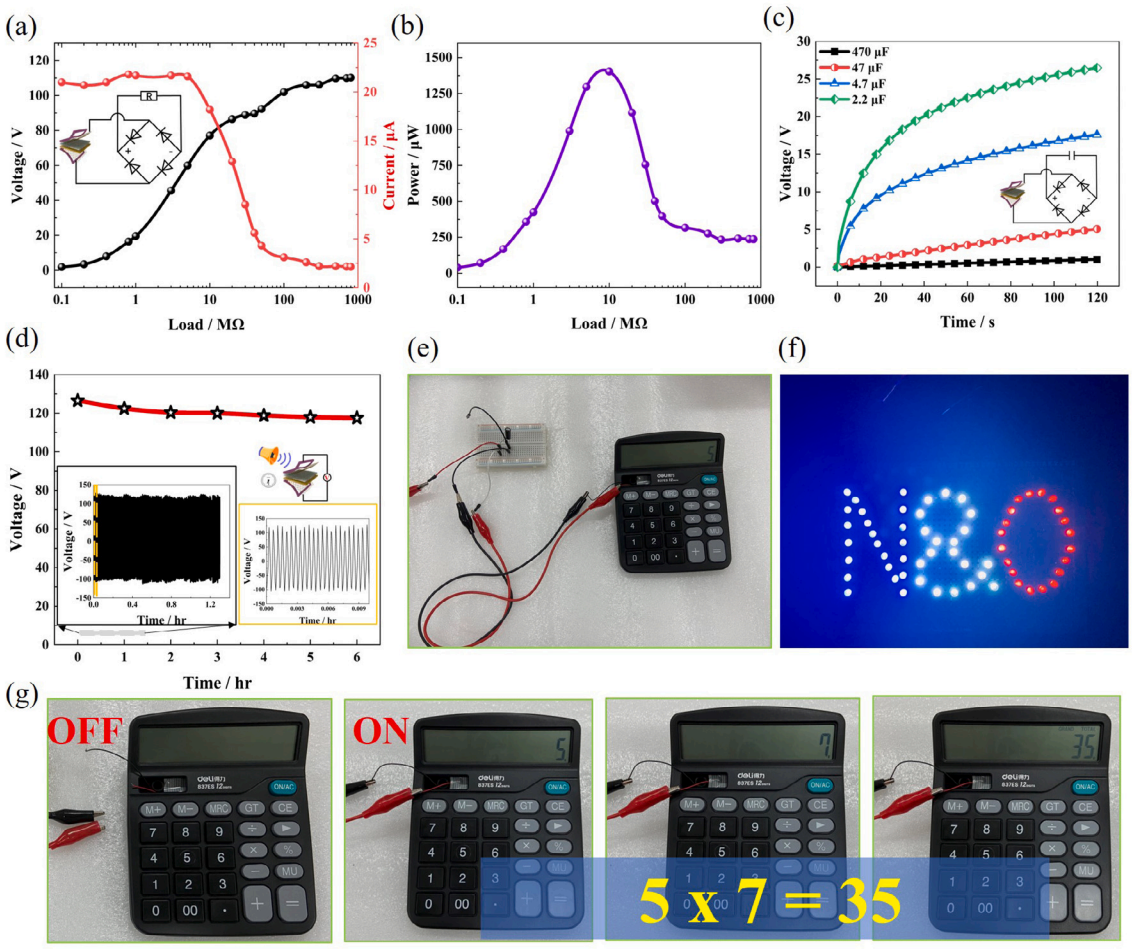

Fig. 4. Nanocomposite acoustic NFM TENGs containing PAN-PVDF-MWCNTs (1 wt%) components: (a) output voltage and corresponding current and (b) output power, under varying external loads. (c) output voltage variations over time for capacitors with different capacitance values. (d) the durability test and ageing effect of NFM TENGs. (e) a calculator powered by the capacitor after electric charging. (f) 62 LEDs powered in series. (g) continuous calculation function powered by the acoustic NFM TENG.

1:1 through a series of experimental studies. Supplementary Figures S1 and S2 illustrate the micro-structure distribution of various nanofibers inside the NFMs, which may be closely related to the aforementioned findings. It is observed that the nanofiber distributions of the optimised NFM tend to be more uniform and have a larger fibre diameter, which may be the reason for the greater electrical output seen in Fig. 2 (c) and 2 (d).

Acoustic waves with various sound pressure levels (SPLs) can propagate in the ambient environment. Consequently, after identifying the ideal weight percentage of the NFM with PAN-PVDF-MWCNTs nanocomponents, the open-circuit voltage of NFM TENGs with PAN-PVDF-MWCNT components under varying excitation acoustic frequency is shown in Figure S9 in Supplementary. The electric output of NFM TENG is maximum at around 200 Hz. Then, the electrical outputs of the NFM TENG at multiple SPLs were evaluated at a constant frequency of 200 Hz. Both the open-circuit voltage V_{oc} and the short-circuit current I_{sc} grew as the SPL increased in Fig. 3 (a) and (b). Specifically, I_{sc} increased from 0.4 μA to 30.2 μA as V_{oc} increased from 3 V to 126.5 V, which corresponded to an increase in SPL from 86 dB to 116 dB. In addition, when the SPL exceeded 102 dB, it was observed that both V_{oc} and I_{sc} rose quickly and exhibited a linear relation with SPL, as given in Figure S6 of Supplementary. Figure S10 in Supplementary also shows the open-circuit voltage of PAN-PVDF-MWCNT (1 wt%) NFM TENGs for various distance to the end of acoustic impedance tube and their corresponding SPLs. The effects of the NFM thickness on electrical outputs of the acoustic NFM TENG were also explored. The open-circuit voltage V_{oc} and short-circuit current I_{sc} were found to decrease as the NFM thickness increased, see Fig. 3 (c) and (d). Consequently, in order to optimise performance, the NFM thickness should be as small as possible. However, it was found that the NFMs were susceptible to fatigue and rupture when the thickness was less than 20 μm. Thus the ideal thickness of NFM in this study was determined to be roughly 20 μm.

The electrical output of an acoustic NFM TENG containing PAN-PVDF-MWCNTs (1 wt%) components was next studied using various external electrical loads. Alternating voltage and current generated by the acoustic TENG were rectified and then assessed using external resistors with varying resistances. Fig. 4 (a) and 4 (b) illustrate the output voltage, current and power under varying external loads. The output voltage rose from 1.9 V to 110.3 V when the resistance was increased from 0.1 MΩ to 1000 MΩ, whereas the output current exhibited a reverse trend. As illustrated in Fig. 4 (b), the peak output power achieved was 1.41 mW with an external load of around 10 MΩ. This power density compares favourably with data from the literature, see Fig. 5.

For the purpose of determining the charging capacity of the acoustic NFM TENG, various capacitors were chosen as the power storage units for energy harvesting performance tests. As indicated in Fig. 4 (c), the charged voltage of 2.2 μF, 4.7 μF, 47 μF, and 470 μF capacitors reached 26.5 V, 17.6 V, 5.06 V and 1.02 V, respectively, after 120 s of charging

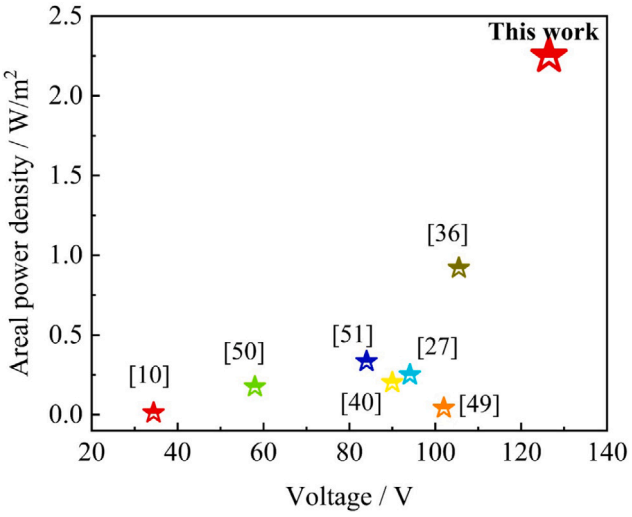

Fig. 5. Comparison of electric outputs between current work and literature.

at SPL of 116 dB. As may be expected, smaller capacitors generally reached greater voltages. The lifespan test of the NFM TENGs (PAN-PVDF-MWCNTs (1 wt%)) was conducted for a total of 6 h under the acoustic excitation of 116 dB at 200 Hz. The electric output data were continuously recorded for 1.3 h, after which the open-circuit voltage was checked every hour to minimise data storage capacity. In general, the open-circuit voltage of the NFM TENG remains as high as 120 V after six hours of operation, as shown in Fig. 4 (d). The acoustic NFM TENG with an integrated capacitor can be considered a self-powered system: after 120 s of charging, the 2.2 μF capacitor can power a digital calculator for a few seconds, see Fig. 4 (e). Meanwhile, with the help of a rectifying circuit, the acoustic NFM TENG device can illuminate 62 commercial LEDs (Fig. 4 (f) and Video 1 in Supplementary) and power a calculator (Fig. 4 (g) and Video 2 in Supplementary) performing regular calculation under the continuous stimulation of sound waves. These preliminary findings suggest that the acoustic NFM TENG can generate sufficient electrical output to power small microelectronic devices. The TENGs also have the advantage of being compact and lightweight (see Figure S13 in Supplementary).

4. Conclusions

In this work, an ultralight, ultrathin and compact NFM TENG has been designed for harvesting acoustic energy with a high specific power. The whole structure is constructed as a periodic contact-separation sandwich device with copper meshes, PET outside frames, a PLA spacer, and an NFM. Compared to single-material NFMs, the novel combination of PAN, PVDF, and MWCNTs in nanocomposite NFMs can significantly improve their ability to convert acoustic energy to electric outputs. Experimental work has also discovered an optimum concentration ratio of the three nanocomponents and the optimal thickness of the nanocomposite NFM for maximising electrical output. When stimulated by sound waves at 116 dB and 200 Hz, the resulting TENG generated a maximum voltage and current output of 126.5 V and 30.2 μA, respectively, and areal power density of 2.25 W/m^2. This is far superior to the performance of single-layer PVDF-based TENGs previously reported. By using rectification and storage, the potential of the TENG to power digital devices was demonstrated, indicating an opportunity for use in microelectronic devices and the Internet of Things.

CRediT authorship contribution statement

Wenhao Sun: Conceptualization, Investigation, Methodology, Software, Validation, Visualization, Writing – original draft, Writing – review & editing. **Guosheng Ji:** Conceptualization, Investigation, Methodology, Software, Validation, Visualization, Writing – original draft, Writing – review & editing. **Junli Chen:** Software, Investigation. **Dan Sui:** Resources, Project administration, Writing – review & editing. **Jie Zhou:** Conceptualization, Supervision, Funding acquisition, Resources, Project administration, Writing – review & editing. **John Huber:** Conceptualization, Supervision, Project administration, Writing – review & editing.

Declaration of competing interest

The authors declare that they have no known competing financial interests or personal relationships that could have appeared to influence the work reported in this paper.

Data availability

Data will be made available on request.

Acknowledgements

Wenhao Sun, Junli Chen, Dan Sui and Jie Zhou are grateful for the financial support from the National Natural Science Foundation of China (Grant No. 12072277) and the Fundamental Research Funds for the Central Universities of China (Grant No. G2022KY0608). Guosheng Ji is supported by the Clarendon Fund and Trinity College Scholarship at the University of Oxford, UK.

Appendix A. Supplementary data

Supplementary material related to this article can be found online at https://doi.org/10.1016/j.nanoen.2023.108248.

References

[1] J.D. Miller, Effects of noise on people, J. Acoust. Soc. Am. 56 (3) (1974) 729–764.
[2] Y. Tao, M. Ren, H. Zhang, T. Peijs, Recent progress in acoustic materials and noise control strategies–a review, Appl. Mater. Today 24 (2021) 101141.
[3] H.P. Lee, S. Kumar, S. Garg, K.M. Lim, Assessment of in-cabin noise of wide-body aircrafts, Appl. Acoust. 194 (2022) 108809.
[4] G. Ji, J. Xu, J. Zhou, W. Kang, The exploration of transmission property by using the circular-interface types of porous acoustic metamaterials, Int. J. Mech. Sci. 230 (2022) 107558.
[5] W. Sun, B. Pan, X. Song, H. Xiao, J. Zhou, D. Sui, A novel sound absorber design of nanofibrous composite porous material, Mater. Des. 214 (2022) 110418.
[6] T. Yuan, X. Song, J. Xu, B. Pan, D. Sui, H. Xiao, J. Zhou, Tunable acoustic composite metasurface based porous material for broadband sound absorption, Compos. Struct. 298 (2022) 116014.
[7] X. Fan, J. Chen, J. Yang, P. Bai, Z. Li, Z.L. Wang, Ultrathin, rollable, paper-based triboelectric nanogenerator for acoustic energy harvesting and self-powered sound recording, ACS Nano 9 (4) (2015) 4236–4243.
[8] Z. Yu, Y. Zhang, Y. Wang, J. Zheng, Y. Fu, D. Chen, G. Wang, J. Cui, S. Yu, L. Zheng, et al., Integrated piezo-tribo hybrid acoustic-driven nanogenerator based on porous MWCNTs/PVDF-TrFE aerogel bulk with embedded PDMS tympanum structure for broadband sound energy harvesting, Nano Energy 97 (2022) 107205.
[9] G. Ji, J. Huber, Recent progress in acoustic metamaterials and active piezoelectric acoustic metamaterials-a review, Appl. Mater. Today (2021) 101260.
[10] Y. Li, S. Xiao, Y. Luo, S. Tian, J. Tang, X. Zhang, J. Xiong, Advances in electrospun nanofibers for triboelectric nanogenerators, Nano Energy (2022) 107884.
[11] S.N. Cha, J.-S. Seo, S.M. Kim, H.J. Kim, Y.J. Park, S.-W. Kim, J.M. Kim, Sound-driven piezoelectric nanowire-based nanogenerators, Adv. Mater. 22 (42) (2010) 4726–4730.
[12] J. Yang, J. Chen, Y. Liu, W. Yang, Y. Su, Z.L. Wang, Triboelectrification-based organic film nanogenerator for acoustic energy harvesting and self-powered active acoustic sensing, ACS Nano 8 (3) (2014) 2649–2657.

[13] W. Kang, L. Chang, J. Huber, Investigation of mechanical energy harvesting cycles using ferroelectric/ferroelastic switching, Nano Energy 93 (2022) 106862.
[14] K. Xia, Z. Zhu, H. Zhang, C. Du, Z. Xu, R. Wang, Painting a high-output triboelectric nanogenerator on paper for harvesting energy from human body motion, Nano Energy 50 (2018) 571–580.
[15] K. Xia, D. Wu, J. Fu, N.A. Hoque, Y. Ye, Z. Xu, A high-output triboelectric nanogenerator based on nickel–copper bimetallic hydroxide nanowrinkles for self-powered wearable electronics, J. Mater. Chem. A 8 (48) (2020) 25995–26003.
[16] K. Xia, J. Fu, Z. Xu, Multiple-frequency high-output triboelectric nanogenerator based on a water balloon for all-weather water wave energy harvesting, Adv. Energy Mater. 10 (28) (2020) 2000426.
[17] F.U. Khan, Izhar, Hybrid acoustic energy harvesting using combined electromagnetic and piezoelectric conversion, Rev. Sci. Instrum. 87 (2) (2016) 025003.
[18] M. Yuan, Z. Cao, J. Luo, X. Chou, Recent developments of acoustic energy harvesting: A review, Micromachines 10 (1) (2019) 48.
[19] C. Fei, X. Liu, B. Zhu, D. Li, X. Yang, Y. Yang, Q. Zhou, AlN piezoelectric thin films for energy harvesting and acoustic devices, Nano Energy 51 (2018) 146–161.
[20] S.K. Karan, S. Maiti, J.H. Lee, Y.K. Mishra, B.B. Khatua, J.K. Kim, Recent advances in self-powered tribo-/piezoelectric energy harvesters: all-in-one package for future smart technologies, Adv. Funct. Mater. 30 (48) (2020) 2004446.
[21] T. Li, Z. Wang, H. Xiao, Z. Yan, C. Yang, T. Tan, Dual-band piezoelectric acoustic energy harvesting by structural and local resonances of Helmholtz metamaterial, Nano Energy 90 (2021) 106523.
[22] C.-S. Park, Y.C. Shin, S.-H. Jo, H. Yoon, W. Choi, B.D. Youn, M. Kim, Two-dimensional octagonal phononic crystals for highly dense piezoelectric energy harvesting, Nano Energy 57 (2019) 327–337.
[23] M. Safaei, H.A. Sodano, S.R. Anton, A review of energy harvesting using piezoelectric materials: state-of-the-art a decade later (2008–2018), Smart Mater. Struct. 28 (11) (2019) 113001.
[24] N. Sezer, M. Koç, A comprehensive review on the state-of-the-art of piezoelectric energy harvesting, Nano Energy 80 (2021) 105567.
[25] C. Lang, J. Fang, H. Shao, X. Ding, T. Lin, High-sensitivity acoustic sensors from nanofibre webs, Nature Commun. 7 (1) (2016) 1–7.
[26] C. Lang, J. Fang, H. Shao, H. Wang, G. Yan, X. Ding, T. Lin, High-output acoustoelectric power generators from poly (vinylidenefluoride-co-trifluoroethylene) electrospun nano-nonwovens, Nano Energy 35 (2017) 146–153.
[27] W. Wang, Y. Zheng, X. Jin, Y. Sun, B. Lu, H. Wang, J. Fang, H. Shao, T. Lin, Unexpectedly high piezoelectricity of electrospun polyacrylonitrile nanofiber membranes, Nano Energy 56 (2019) 588–594.
[28] H. Shao, H. Wang, Y. Cao, X. Ding, R. Bai, H. Chang, J. Fang, X. Jin, W. Wang, T. Lin, Single-layer piezoelectric nanofiber membrane with substantially enhanced noise-to-electricity conversion from endogenous triboelectricity, Nano Energy 89 (2021) 106427.
[29] W. Kang, J.E. Huber, Prospects for energy harvesting using ferroelectric/ferroelastic switching, Smart Mater. Struct. 28 (2) (2019) 024002.
[30] X. Wang, J. Song, J. Liu, Z.L. Wang, Direct-current nanogenerator driven by ultrasonic waves, Science 316 (5821) (2007) 102–105.
[31] F. Chen, Y. Wu, Z. Ding, X. Xia, S. Li, H. Zheng, C. Diao, G. Yue, Y. Zi, A novel triboelectric nanogenerator based on electrospun polyvinylidene fluoride nanofibers for effective acoustic energy harvesting and self-powered multifunctional sensing, Nano Energy 56 (2019) 241–251.
[32] C. Wu, A.C. Wang, W. Ding, H. Guo, Z.L. Wang, Triboelectric nanogenerator: a foundation of the energy for the new era, Adv. Energy Mater. 9 (1) (2019) 1802906.
[33] Z. Niu, W. Cheng, M. Cao, D. Wang, Q. Wang, J. Han, Y. Long, G. Han, Recent advances in cellulose-based flexible triboelectric nanogenerators, Nano Energy 87 (2021) 106175.
[34] S. Bairagi, G. Khandelwal, X. Karagiorgis, S. Gokhool, C. Kumar, G. Min, D.M. Mulvihill, High-Performance triboelectric nanogenerators based on commercial textiles: Electrospun Nylon 66 nanofibers on silk and PVDF on polyester, ACS Appl. Mater. Interfaces 14 (39) (2022) 44591–44603.
[35] W. Xu, J. Guo, H. Wen, X. Meng, H. Hong, J. Yuan, J. Gao, D. Liu, Q. Ran, Y. Wang, et al., Laminated triboelectric acoustic energy harvester based on electrospun nanofiber towards real-time noise decibel monitoring, Nano Energy (2022) 107348.
[36] H. He, J. Guo, B. Illés, A. Géczy, B. Istók, V. Hliva, D. Török, J.G. Kovács, I. Harmati, K. Molnár, Monitoring multi-respiratory indices via a smart nanofibrous mask filter based on a triboelectric nanogenerator, Nano Energy 89 (2021) 106418.
[37] S.S.H. Abir, M.U.K. Sadaf, S.K. Saha, A. Touhami, K. Lozano, M.J. Uddin, Nanofiber-based substrate for a triboelectric nanogenerator: High-performance flexible energy fiber mats, ACS Appl. Mater. Interfaces 13 (50) (2021) 60401–60412.
[38] Z. Yu, M. Chen, Y. Wang, J. Zheng, Y. Zhang, H. Zhou, D. Li, Nanoporous PVDF hollow fiber employed piezo–tribo nanogenerator for effective acoustic harvesting, ACS Appl. Mater. Interfaces 13 (23) (2021) 26981–26988.
[39] J. Zheng, Z. Yu, Y. Wang, Y. Fu, D. Chen, H. Zhou, Acoustic core–shell resonance harvester for application of artificial cochlea based on the piezo-triboelectric effect, ACS Nano 15 (11) (2021) 17499–17507.
[40] W. Yang, W. Gong, C. Hou, Y. Su, Y. Guo, W. Zhang, Y. Li, Q. Zhang, H. Wang, All-fiber tribo-ferroelectric synergistic electronics with high thermal-moisture stability and comfortability, Nature Commun. 10 (1) (2019) 1–10.
[41] S.S. Rana, M.T. Rahman, S. Sharma, M. Salauddin, S.H. Yoon, C. Park, P. Maharjan, T. Bhatta, J.Y. Park, Cation functionalized nylon composite nanofibrous mat as a highly positive friction layer for robust, high output triboelectric nanogenerators and self-powered sensors, Nano Energy 88 (2021) 106300.
[42] N. Cui, L. Gu, J. Liu, S. Bai, J. Qiu, J. Fu, X. Kou, H. Liu, Y. Qin, Z.L. Wang, High performance sound driven triboelectric nanogenerator for harvesting noise energy, Nano Energy 15 (2015) 321–328.
[43] J. Liu, N. Cui, L. Gu, X. Chen, S. Bai, Y. Zheng, C. Hu, Y. Qin, A three-dimensional integrated nanogenerator for effectively harvesting sound energy from the environment, Nanoscale 8 (9) (2016) 4938–4944.
[44] H. Zhao, X. Xiao, P. Xu, T. Zhao, L. Song, X. Pan, J. Mi, M. Xu, Z.L. Wang, Dual-tube Helmholtz resonator-based triboelectric nanogenerator for highly efficient harvesting of acoustic energy, Adv. Energy Mater. 9 (46) (2019) 1902824.
[45] W. Qiu, Y. Feng, N. Luo, S. Chen, D. Wang, Sandwich-like sound-driven triboelectric nanogenerator for energy harvesting and electrochromic based on Cu foam, Nano Energy 70 (2020) 104543.
[46] Y. Cao, H. Shao, H. Wang, X. Li, M. Zhu, J. Fang, T. Cheng, T. Lin, A full-textile triboelectric nanogenerator with multisource energy harvesting capability, Energy Convers. Manage. 267 (2022) 115910.
[47] C. Chen, Z. Wen, J. Shi, X. Jian, P. Li, J.T. Yeow, X. Sun, Micro triboelectric ultrasonic device for acoustic energy transfer and signal communication, Nature Commun. 11 (1) (2020) 1–9.
[48] S. Lee, J.-W. Park, Fingerprint-inspired triboelectric nanogenerator with a geometrically asymmetric electrode design for a self-powered dynamic pressure sensor, Nano Energy 101 (2022) 107546.
[49] K. Mālnieks, P. Kaufelde, A. Linarts, L. Lapčinskis, O. Verners, A. Šutka, Triboelectric laminates from polydimethylsiloxane bilayers for acoustic energy harvesting, Mater. Lett. 329 (2022) 133188.
[50] C. Zhao, D. Liu, Y. Wang, Z. Hu, Q. Zhang, Z. Zhang, H. Wang, T. Du, Y. Zou, H. Yuan, et al., Highly-stretchable rope-like triboelectric nanogenerator for self-powered monitoring in marine structures, Nano Energy 94 (2022) 106926.
[51] Y. Zhou, X. Tao, Z. Wang, M. An, K. Qi, K. Ou, J. He, R. Wang, X. Chen, Z. Dai, Electret-doped polarized nanofiber triboelectric nanogenerator with enhanced electrical output performance based on a micro-waveform structure, ACS Appl. Electron. Mater. (2022).
[52] H. Shao, H. Wang, Y. Cao, X. Ding, J. Fang, H. Niu, W. Wang, C. Lang, T. Lin, Efficient conversion of sound noise into electric energy using electrospun polyacrylonitrile membranes, Nano Energy 75 (2020) 104956.
[53] S.K. Singh, P. Kumar, R. Magdum, U. Khandelwal, S. Deswal, Y. More, S. Muduli, R. Boomishankar, S. Pandit, S. Ogale, Seed Power: Natural seed and electrospun poly(vinyl difluoride)(PVDF) nanofiber based triboelectric nanogenerators with high output power density, ACS Appl. Bio Mater. 2 (8) (2019) 3164–3170.
[54] A.M. Mohamed, K. Yao, Y.M. Yousry, J. Wang, S. Ramakrishna, Open-cell P(VDF-TrFE)/MWCNT nanocomposite foams with local piezoelectric and conductive effects for passive airborne sound absorption, J. Appl. Phys. 127 (21) (2020) 214102.
[55] H. Yu, T. Huang, M. Lu, M. Mao, Q. Zhang, H. Wang, Enhanced power output of an electrospun PVDF/MWCNTs-based nanogenerator by tuning its conductivity, Nanotechnology 24 (40) (2013) 405401.
[56] E.C. Statharas, K. Yao, M. Rahimabady, A.M. Mohamed, F.E.H. Tay, Polyurethane/poly(vinylidene fluoride)/MWCNT composite foam for broadband airborne sound absorption, J. Appl. Polym. Sci. 136 (33) (2019) 47868.

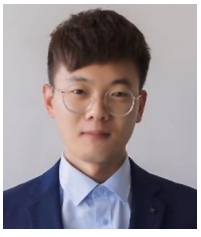

Wenhao Sun is currently a Ph.D. candidate in Prof. Jie Zhou's team at the School of Aeronautics, Northwestern Polytechnical University. His research mainly focuses on the developing novel nanofiber-based acoustic energy harvester devices and acoustic porous piezoelectric material design.

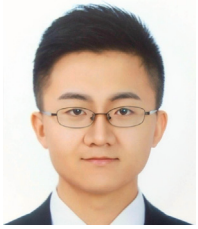

Guosheng Ji is currently a Ph.D. candidate at the Department of Engineering Science, University of Oxford. He obtained his MPhil degree in Mechanical Engineering and bachelor's degree in Flying Vehicle Power Engineering at the Hong Kong University of Science and Technology and Beijing University of Aeronautics and Astronautics, respectively. His current research aims to develop piezoelectric acoustic metamaterials for both noise reduction and energy harvesting.

Junli Chen is currently a Ph.D. student studying in the team of Prof. Jie Zhou at the School of Aeronautics, Northwestern Polytechnical University. He mainly focuses on researching bio-inspired low-noise flapping-wing micro air vehicles based on nano-fibrous membrane wings.

Dan Sui received her Ph.D. degree from the Department of Engineering Science at the University of Oxford in 2015. She is currently an Associate Research Fellow at the School of Aeronautics at Northwestern Polytechnical University. Her research interests include functional piezoelectric and ferroelectric materials, bionic acoustic structure design and preparation and characterisation of electrospun materials.

Jie Zhou is currently a Professor at the School of Aeronautics at Northwestern Polytechnical University. He received his Ph.D. degree in the Faculty of Engineering and Environment at the University of Southampton, in 2014. His research interests include functional nanofibrous materials, acoustic energy harvesting, acoustic metamaterial, and novel bio-acoustical structure design.

John Huber is an Associate Professor in the Department of Engineering Science and a tutorial fellow at Oriel College at the University of Oxford. He studied engineering at Cambridge University and gained a Ph.D. researching mechanics of materials. Joining Oxford Engineering Science in 2005, he continued to research smart materials for actuators and sensors along with other topics in the mechanics of materials.